

See discussions, stats, and author profiles for this publication at: <https://www.researchgate.net/publication/272678753>

Hydrodynamic Perspective on Asphaltene Agglomeration and Deposition

ARTICLE *in* ENERGY & FUELS · FEBRUARY 2015

Impact Factor: 2.79 · DOI: 10.1021/ef501931h

READS

163

4 AUTHORS, INCLUDING:



[L. M. Portela](#)

Delft University of Technology

47 PUBLICATIONS 653 CITATIONS

[SEE PROFILE](#)



[Aris Twerda](#)

Delft University of Technology

9 PUBLICATIONS 15 CITATIONS

[SEE PROFILE](#)



[R.A.W.M. Henkes](#)

Delft University of Technology

74 PUBLICATIONS 1,064 CITATIONS

[SEE PROFILE](#)

Hydrodynamic Perspective on Asphaltene Agglomeration and Deposition

Koen C. J. Schutte,^{*†} Luis M. Portela,[†] Aris Twerda,^{‡,||} and Ruud A. W. M. Henkes[‡]

[†]Department of Chemical Engineering, Delft University of Technology, Post Office Box 5, 2600 AA Delft, The Netherlands

[‡]Process & Energy Department, Delft University of Technology, Post Office Box 5, 2600 AA Delft, The Netherlands

^{||}TNO, Post Office Box 155, 2600 AD Delft, Netherlands

Supporting Information

ABSTRACT: In this work, we propose a detailed numerical model for asphaltene agglomeration and deposition, as induced by a resolved turbulent liquid carrier phase flow, in which transport, breakup, and re-entrainment are also taken into account. Asphaltene phase separation is represented by the appearance of adhesive primary particles, which bond upon collision and act as a precursor to agglomerate formation. Deposition is considered using a novel approach in the context of agglomerate structure resolving simulations: the attractive particle–wall interaction is modeled by a damped harmonic oscillator, whereas the deceleration of depositing particles occurs with a characteristic relaxation time. In the absence of deposition, agglomeration and breakup give rise to a statistical steady state. Universal scaling relations, valid for a large range of Reynolds numbers, accurately predict the mean agglomerate mass in this steady state. We show that the shape of the agglomerates is insensitive to the breakup mechanism considered and that the fractal dimension is similar to experimental values reported in the literature for asphaltenes. It is found that the properties of the agglomerates change when two-way coupling is considered instead of one-way coupling, but not when large-eddy simulations are conducted instead of direct numerical simulations. When particle–wall interactions are included, deposition predominantly occurs close to the region where asphaltene phase separation takes place. The morphology of the deposit layer is shown to depend upon the local concentration and the mobility of the deposited particles; we also present how these features depend upon the parameters of the deposition model.

INTRODUCTION

Asphaltene deposition is a major cause for flow obstructions encountered during hydrocarbon production.¹ Historically, asphaltene-related research has mainly been focused on elucidating the complex molecular structure of this heavy crude oil fraction as well as on constructing thermodynamic models that describe the phase separation of asphaltenes from a crude oil under laboratory or production conditions. Although asphaltene phase separation is a necessary though insufficient condition for the formation of asphaltene deposits, the first literature on the actual formation of asphaltene agglomerates and deposits under flow conditions has emerged only in the recent past. As such, it is now known that asphaltenes can form porous, fractal aggregates after phase separation, with typical dimensions that have been measured to grow from a few² up to several hundreds of micrometers.³

Most of the models for asphaltene aggregation proposed in the literature^{2–5} are based on population balance equations, in which the formation (and, if considered, breakup) of asphaltene agglomerates are studied in an Eulerian context (viz., by monitoring global properties of the agglomerate population, such as the concentration as a function of the agglomerate size), using collision and breakup kernels to account for the interactions between agglomerates. Asphaltene deposition is typically modeled in the literature using empirical correlations for the deposition of spherical particles from laminar or turbulent flows. One example of such an approach is given by the work of Escobedo and Mansoori⁶ (who were early adopters of modeling the deposition of asphaltenes, with their first

contributions dating back to 1995); they studied the deposition rate of spherical particles from a turbulent flow as a function of the particle diameter, modeling the particle deposition by Fick's law of diffusion, corrected for the particle inertia. Another simple deposition model based on empirical relations for mass transport in turbulent flows was constructed by Jamialahmadi et al.,⁷ the parameters of this model were fitted to experimental data on the asphaltene deposit layer thickness obtained by thermal conductance measurements in a stainless-steel pipe. Ramirez-Jaramillo et al.⁸ proposed a model in which molecular diffusion is assumed to be the driving force for the deposition of asphaltene particles in oil production pipelines, combined with a shear removal term to account for re-entrainment. Vargas et al.⁹ used a pseudo-first-order reaction mechanism to account for the formation of deposits out of asphaltenes that are transported to the walls of the flow domain by a diffusion-driven process, considering convective transport in the streamwise direction. Finally, Akbarzadeh et al.¹⁰ studied the deposition of asphaltenes from live crude oils under the influence of pressure depletion, in a turbulent Couette flow cell. The results of these measurements were used to determine parameters for a model that predicts asphaltene deposition as a

Special Issue: 15th International Conference on Petroleum Phase Behavior and Fouling

Received: August 29, 2014

Revised: January 16, 2015



result of Brownian motion, turbulent transport, and turbophoresis, combined with a shear removal mechanism to account for re-entrainment.

Even though the Eulerian models discussed above are very efficient and, thus, very useful for studying deposition and re-entrainment in full-scale systems, a proper understanding of the underlying physics of these processes is required for defining proper closure relations in such models. Therefore, it is also very instructive to study agglomeration, breakup, deposition, and re-entrainment on the level of individual particles and agglomerates (the so-called Lagrangian approach). The work of Boek et al.¹¹ is an example in which a Lagrangian method is used to consider the asphaltene–flow interactions from first principles. In that work, the deposition of asphaltenes in glass capillaries is studied, both experimentally and numerically. In the numerical model, stochastic rotation dynamics are used to explicitly solve for the flow inside the capillary, whereas the asphaltene–asphaltene interaction and the asphaltene–wall interaction are taken into account by screened Coulomb potentials.

The formation and breakup of agglomerates is also frequently studied in other fields of science and engineering. Restricting this overview to Lagrangian methods, typically, agglomerates are represented by equivalent spherical entities in the models that were developed to this end, thereby not accounting for their internal structure (e.g., Ho and Sommerfeld¹²). Models that do take into account the full spatial structure of agglomerates throughout the agglomerate life cycles are reported more scarcely in the literature, but a few examples do exist. Richardson¹³ studied the formation of particle agglomerates in an astrophysical system, considering three possible outcomes for a collision event: coagulation, restitution, and fragmentation. When coagulating, the colliding primary particles are joined by a rigid bond, such that the formation of complete agglomerate structures can be monitored over time. In a later work, Perrine et al.¹⁴ applied an extended version of this model, which considers two mechanisms of agglomerate breakup: particles are either liberated from preformed agglomerates by the event of a high-speed impact of another agglomerate, or when the relative accelerations of primary particles induce stresses that surpass the strength of the bonds that keep the particles attached to the agglomerate. A model for the aggregation of icy particles in the early stages of asteroid formation was developed by Mäkinen.¹⁵ In this model, particle collisions are considered to result in agglomeration if the relative kinetic energy of the colliding particles is fully dissipated within the time that the individual particles are in contact with each other. Fragmentation of agglomerates is considered using a comprehensive analysis of induced internal stresses in all interparticle bonds. Bonds are broken if either of the internal stress components exceeds the maximum stress that the bond can withstand; this strength is assumed to be proportional to the area of overlap between the particles. Chen and Doi,¹⁶ finally, studied the dissociation of aggregating colloids in strongly sheared flows. Their model considers that sticky particles can roll over each other without slipping at their contact point; also in this model, bonds between particles are considered to break when the induced stresses exceed the strength of those bonds.

The basic structure of the agglomeration and breakup modules considered in this work is similar to models proposed by Richardson, Mäkinen, and Chen and Doi; however, a major difference is that, in contrast to the former authors, in our work,

we study a turbulent flow as the driving force for the agglomeration and deposition of primary particles that emerge from a phase separation process.

Problem Formulation. As a next step toward a better understanding of the agglomeration and deposition of asphaltenes under macroscopic flow conditions, in this work, we propose an advanced numerical model for the transport, agglomeration, breakup, deposition, and re-entrainment of asphaltenes, as induced by the flow. In contrast to earlier models proposed for asphaltene agglomeration and deposition under turbulent flow conditions, the agglomerate structure is explicitly accounted for in our model. In the end, the results obtained in this ongoing research can be used to construct improved engineering models that predict whether and where asphaltene deposits will be formed, as well as to evaluate strategies to mitigate this deposition.

The remainder of this paper is organized as follows. In the next section, the model proposed in this work is explained in more detail. Thereafter, we describe the simulated cases, followed by a discussion of the results of the simulations. Finally, conclusions are drawn, and we outline the next steps that will be taken in our research.

THEORETICAL BASIS

The dispersed-phase model developed in this work is implemented as an extension of an existing, validated, particle-laden channel flow code. In essence, the dispersed-phase solver only interacts with the continuous-phase solver by virtue of velocity and force-field interpolations, making the implementation very portable; adapting the model to work with different flow solvers, provided that those can provide temporal and spatial velocity information, is straightforward.

The solver for the turbulent liquid carrier phase uses a finite-volume spatial discretization scheme, combined with second-order Adams–Bashforth time integration and the predictor–corrector method to solve the incompressible Navier–Stokes equations; it is capable of operating in both direct numerical simulation (DNS) and large-eddy simulation (LES) modes. In LES mode, the Smagorinsky model, together with van Driest damping of the eddy viscosity near the walls, is applied to account for the sub-grid turbulence scales; this is a simple model, known to perform well for channel flows. The maximum admissible time step for the continuous-phase solver is determined using the Courant criterion. Further details of the original code can be found in the studies by Portela and Oliemans¹⁷ and Li et al.¹⁸

In addition to our previous study,¹⁹ in which the forces exerted by the dispersed phase on the turbulent liquid carrier phase were neglected (one-way coupling), here, we also consider two-way coupled simulations, in which these forces are taken into account in the fluid-phase momentum equations. Because we study relatively small mass fractions for the dispersed phase in this work, the influence of the particles on the mass conservation equation for the fluid can safely be neglected.

Phase Separation. We consider primary particles to act as a precursor to agglomerate and deposit formation. The phase separation of asphaltenes from the crude oil is considered to mark a transition from a stable state, in which no macroscopic agglomeration can take place, to a situation in which asphaltene particles are formed that subsequently start to agglomerate. In the context of our model, the phase transition thus corresponds to a sudden appearance of primary particles, which are considered to be spherical and are described as point particles with a finite radius. In this so-called point-particle approach, the interaction between the continuous and dispersed phases is described by considering only flow properties at the location of the center of the primary particles.

Hydrodynamic Force Model. The only forces acting on the dispersed phase considered in this work are the drag force and the added mass effect. The drag force is approximated using Stokes drag, without accounting for shielding effects for primary particles that are

close to each other (the “free-draining” approximation). Because of the high local particle concentration inside the agglomerates, shielding effects in reality are likely to have a substantial impact on the force exerted on the primary particles; for simplicity, however, this effect is neglected in this work. Although the Stokes drag approximation strictly only holds for particle Reynolds numbers much smaller than unity (and typical values of the particle Reynolds number in our work are between 0 and 10), we do not apply a correction to it, to preserve the linearity of the drag force. Consequently, the drag force on individual primary particles will be underestimated, thereby compensating (to some extent) for the overestimation of the hydrodynamic force resulting from the free-draining approximation.

Considering Stokes drag and the added mass force, the equation of motion of a single, spherical particle is given by (see, e.g., Hollander et al.²⁰)

$$\rho_p \frac{4\pi R_p^3}{3} \frac{d\mathbf{U}_p}{dt} = \mathbf{F}_p = \underbrace{6\pi\eta_f R_p (\mathbf{U}_f - \mathbf{U}_p)}_{\text{drag}} + \underbrace{\frac{\rho_f}{2} \frac{4\pi R_p^3}{3} \left(\frac{d\mathbf{U}_f}{dt} - \frac{d\mathbf{U}_p}{dt} \right)}_{\text{added mass}} \quad (1)$$

where ρ_p and ρ_f denote the dispersed- and continuous-phase densities, respectively, η_f denotes the fluid viscosity, R_p denotes the radius of the primary particle, and \mathbf{U}_f denotes the velocity of the continuous phase evaluated at the location of the particle center. Neglecting the material derivative of the fluid velocity in the added mass term, eq 1 reduces to

$$\check{\rho}_p \frac{4\pi R_p^3}{3} \frac{d\mathbf{U}_p}{dt} \equiv \check{\mathbf{F}}_p = 6\pi\eta_f R_p (\mathbf{U}_f - \mathbf{U}_p) \quad (2)$$

with $\check{\rho}_p = \left(\rho_p + \frac{\rho_f}{2} \right)$

where $\check{\rho}_p$ can be seen as the effective dispersed-phase density corrected for the added mass effect.

The expression for $\check{\mathbf{F}}_p$ given in eq 2 is used to describe the hydrodynamic force acting on any single primary particle (both unbounded particles and particles that are part of agglomerates), and $\check{\rho}_p$ substitutes ρ_p when calculating the mass of primary particles and/or agglomerates. Rewriting this last equation, one can arrive at an expression for the particle relaxation time τ_p (a measure for how quickly a particle can adapt to changes in the local fluid velocity):

$$\frac{d\mathbf{U}_p}{dt} = \frac{1}{\tau_p} (\mathbf{U}_f - \mathbf{U}_p) \quad \text{where} \quad \tau_p = \frac{2\check{\rho}_p R_p^2}{9\eta_f} \quad (3)$$

We are interested in simulating upward vertical flows of systems that have density ratios between the dispersed and continuous phases close to unity. As a result, gravity does not have a component in the wall-normal direction, and the streamwise gravity-induced slip velocity of the particles is negligible when compared to typical turbulent velocity fluctuations. Likewise, it is expected that the influence of the lift force is small, such that this force can also be neglected. We have confirmed that the properties of the steady-state agglomerate population formed in the absence of deposition and re-entrainment do not change when the lift force and the full formulation of the added mass are in fact included in the model, showing that the simplifications made above are reasonable.

Agglomeration. We assume that each collision between primary particles results in the formation of a bond between these particles. This corresponds to assuming that the collision efficiency is equal to unity (“hit-and-stick” approach). Physically, the probability of particles adhering during a collision event depends upon the relative time scales involved in the adhesion process and the particle contact time. Because, in this work, we only consider agglomeration in competition with breakup, the simplification of assuming a 100% collision efficiency seems to be a fair approximation, as, at least to some extent, physically

improper agglomeration events will quickly be undone by the breakup mechanisms.

Colliding particles can be either unbounded or part of an agglomerate that has been formed earlier; for colliding agglomerates, the pair of primary particles that has collided is also identified, thereby keeping track of the internal structure of all agglomerates formed. All collisions between particles and agglomerates are considered to be purely inelastic, conserving both linear and angular momentum (see, for instance, the work of Richardson¹³ for the corresponding equations for the linear and angular velocities of the agglomerate after a collision). The interparticle bonds formed during collisions are considered to have an infinite resistance to deformation, resulting in agglomerates that are rigid up to the point where the bonds between individual particles are broken; the relative position of primary particles inside an agglomerate therefore does not change as long as the agglomerate stays structurally intact.

Agglomerate Equations of Motion. Due to the infinite agglomerate rigidity, the motion of primary particles that constitute an agglomerate results from the laws of solid body motion; it is thus not given by expression 2 itself. The motion of the agglomerates is solved by a superposition of the linear motion of the center of mass of the agglomerate and the rotational motion of the body around this center of mass. The equation for the velocity of the center of mass, \mathbf{U}_{cm} , is given by

$$\check{m}_a \frac{d\mathbf{U}_{cm}}{dt} = \sum \check{\mathbf{F}}_p \quad (4)$$

where the sum runs over all primary particles that constitute the agglomerate, \check{m}_a represents the total mass of the agglomerate ($\check{m}_a = \sum \check{m}_p$, considering also the added mass), and $\check{\mathbf{F}}_p$ denotes the hydrodynamic force that is acting on a particle, as given by eq 2. Similarly, the equation for the angular velocity of the agglomerates is given by

$$\frac{d(\mathbf{I}\Omega)}{dt} = \check{\mathbf{T}} = \sum (\mathbf{r}_p \times \check{\mathbf{F}}_p) \quad (5)$$

where \mathbf{I} represents the moment of inertia tensor of the agglomerate and $\check{\mathbf{T}}$ denotes the total torque. A standard technique for solving expression 5 for objects of general shape, for which the time derivative of \mathbf{I} is non-zero, is employed in this work. It involves transforming eq 5 to a non-inertial frame of reference that is spanned by the eigenvectors of \mathbf{I} (which are the principal axes of inertia of the agglomerate), reducing it to the Euler equations for the rotation of a rigid body. For a more in-depth explanation of this solution strategy as well as the theory of solid-body dynamics in general, the reader is referred to a classical mechanics textbook, for instance the one by Goldstein.²¹

Time Integration. The equations of motion of the agglomerates are integrated using an explicit first-order Euler forward time-integration scheme. At the start of each time step of the dispersed-phase model, the linear and rotational center-of-mass acceleration of all agglomerates are determined using eqs 4 and 5; these accelerations are assumed to be constant throughout the time step. For agglomerates that collide during the time step dt , however, collisions are resolved with sub-time-step temporal accuracy, by splitting the time step for each colliding agglomerate pair such that the momentum exchange takes place at the instant that the primary particles are touching. This is performed to ensure that no excessive artificial overlap of primary particles builds up over time. A synchronized time step is used between the continuous- and dispersed-phase solvers. To ensure stability, the time step is chosen such that it is equal to or smaller than the minimum of (i) the time step dictated by the continuous-flow solver, (ii) half of the relaxation time of a single primary particle, as defined in eq 3, and (iii) the largest value of dt for which any particle present in the domain travels more than half a fluid grid cell per time step, in any given direction. No numerical stability issues were encountered using this setup.

Breakup of Agglomerates. In general, in a rigid body, four principal modes of internal stress, which could result in the breakage of that body, can be distinguished: *straining*, *shearing*, *twisting*, and

bending. Straining is associated with the normal component of the force exerted on the body (or bond), and shearing is related to the tangential force component, whereas twisting and bending are associated with the normal and tangential components of the induced torque, respectively; a schematic representation is given in Figure 1. In

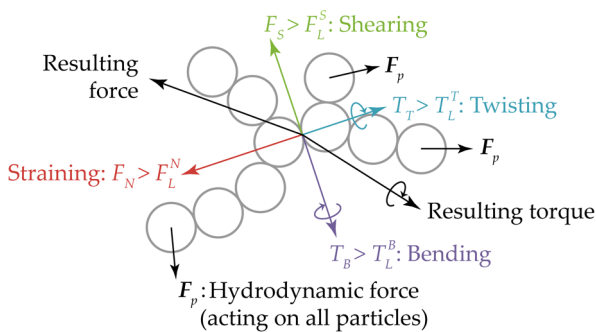


Figure 1. Decomposition of internal stresses induced in interparticle bonds by hydrodynamic forces. F_L^N , F_L^S , T_L^B , and T_L^T denote the maximum straining, shearing, bending, and twisting stresses that bonds can withstand, respectively (viz., the strength of the bonds).

our model, all of these breakup mechanisms are taken into account. The internal stresses in all of the bonds between the primary particles in the agglomerates are computed by considering that the acceleration of each primary particle follows from the rigid-body equations of motion of the agglomerate. Because this acceleration must also result from a balance of forces on acting on that individual primary particle, we can write

$$\frac{d\mathbf{U}_p}{dt} = \frac{d\mathbf{U}_{cm}}{dt} + \frac{d\Omega}{dt} \times \mathbf{r}_p + \Omega \times \frac{d\mathbf{r}_p}{dt} = \frac{1}{m_p} (\mathbf{F}_p + \sum \mathbf{F}_b) \quad (6)$$

where \mathbf{r}_p represents the distance of the primary particle p to the center of mass of the agglomerate, the sums run over all bonds that the particle p has with other primary particles ("nearest neighbors"), and the values of \mathbf{F}_b represent the forces in those bonds. Equating expression 6 for all primary particles in an agglomerate results in a system of n equations. Because we consider agglomerates to be rigid and our model fully resolves agglomerate collisions in time, the probability of two agglomerates colliding at more than one location at the same time is infinitesimally small. As a result, any combination of primary particles that are part of one agglomerate are always connected by one unique pathway only, and in an agglomerate that consists of n particles, exactly $n - 1$ interparticle bonds are present. The number of unknown values of \mathbf{F}_b is thus equal to $n - 1$; hence, the system of equations given by expression 6 can readily be solved. A similar set of equations is solved for the induced torques in the interparticle bonds, and a subsequent geometric decomposition yields the straining (F^N), shearing (F^S), bending (T^B), and twisting (T^T) components of the stress in all bonds between primary particles in the agglomerate.

Bonds are considered to be broken when any of the internal stress components exceed threshold values that are characteristic for the strength of the bonds, provided that the resulting fragments of the agglomerates, that keep their structure after the breakup event, move apart afterward. Although this may seem to be counterintuitive, the latter condition is not necessarily fulfilled if only one particular stress component of an interparticle bond exceeds the breaking strength, because competing stress components could cause the fragments to immediately reattach if the bond is broken. As an example, one can think of a situation in which both a bending moment and a compressive stress are induced in one particular bond at the same time. The bending moment could by itself nominate the bond for breakage, yet the compressive stress may prevent the resulting

agglomerate fragments from truly separating. If multiple bonds in one agglomerate are eligible for breakup at the same instant of time, a random candidate from these bonds is selected to be actually broken, such that one agglomerate is broken in a maximum of two fragments during one time step. The linear and angular velocities of the fragments after breakup are given by conservation of the total linear and angular momentum.

Boundary Conditions at Walls of Flow Domain. At the walls of the flow domain, we consider two types of boundary conditions for the dispersed phase: repulsive and attractive. If no deposition and reentrainment of agglomerates is to be considered, collisions between agglomerates and the walls of the flow domain are resolved in time, and in each collision, the linear and angular velocities of the agglomerates are changed such that the wall-normal velocity component of the primary particle that has collided with the wall is reversed (specular reflection). When adhesive walls are considered, however, resolving the actual deposition is not feasible in the context of the model proposed in this work, since, physically, the interaction range is very small. Instead of resolving microscopic interactions between the walls and particles, a mesoscopic description of the attachment process is needed.

Deposition Model. To the best knowledge of the authors, deposition has never been taken into account before in a structure-revolving Lagrangian agglomeration model. By analogy of the interparticle collision model adapted in this work, an obvious choice for modeling deposition would be to consider that primary particles form bonds with the walls of the flow domain when colliding into them, to assume that these bonds are rigid, and to attribute limiting stresses to the bonds in a similar way as for the interparticle bonds. Initial investigations using such an approach revealed, however, that this model produces unphysical results.

The assumption that rigid bonds are formed between particles and walls of the flow domain prevents agglomerates from reorientating with respect to the walls. Because particles are predominantly transported in the streamwise direction by the continuous carrier phase, such an assumption gives rise to a situation in which the bonds inside deposited agglomerates are mainly in a state of compressive internal stress. As a result, agglomerates can break neither from the wall nor internally considering the breakup formulation implemented in our model. Consequently, upside down "tree"-shaped structures that are attached to (both) wall(s) of the flow domain at their sides are quickly formed. Theoretically, this problem could be solved by relaxing the assumption that particle–wall bonds are infinitely rigid. This would, however, vastly increase the complexity of the breakup algorithm, because multiple primary particles of one agglomerate will eventually come in contact with the walls, violating the assumption that pathways between primary particle pairs in agglomerates are always unique. Therefore, a deposition model along these lines was not further pursued.

Instead, the particle–wall attachment is treated by modeling the walls by interaction potentials rather than solving for the actual collisions of agglomerates with the walls of the flow domain; thereby, particles are not forced to stick instantly upon reaching the coordinates of the walls. Again, making the interaction range very small would result in a very stiff problem, requiring very small time steps, which is an undesirable effect. Instead, we relax the requirement of particles adhering exactly to the wall of the flow domain, by assuming a finite interaction range between the wall and the particles. A damped harmonic oscillator, also known as a spring-dashpot system, acting in the wall-normal direction, is used to account for the attractive interaction between asphaltene particles and the walls of the flow domain

$$\mathbf{F}_{s-d}^{\text{wall}} = -\xi(cW_p \pm k\delta_s)\gamma F_L^N \hat{z} \quad (7)$$

where k and c are spring and damping constants, respectively, W_p represents the wall-normal component of the primary particle velocity, δ_s represents the normal-wise distance from the wall to the face of the particle, and \hat{z} is the unit normal in the direction of the positive wall-normal coordinate. The plus sign corresponds to the bottom wall of

the channel domain, and the minus sign corresponds to the top wall. The parameter γ is a scaling factor that relates the particle–wall interaction force to the particle–particle interaction force, whereas ξ accounts for the finite interaction range between particles and the wall:

$$\xi = \begin{cases} 1.0 & \text{if the center of the particle is inside} \\ & \text{the wall} \\ 1.0 - (\delta_s/R_c)^2 & \text{if the center of the particle is inside} \\ & \text{the flow and } \delta_s < R_c \end{cases} \quad (8)$$

The parameters k and c are related by the so-called damping ratio, which is given by

$$\zeta = \frac{c}{2\sqrt{\dot{m}_p k}} \quad (9)$$

where \dot{m}_p represents the mass of a single primary particle; $\zeta = 1$ corresponds to critical damping.

Of course, deposited agglomerates will slide over the walls of the flow domain indefinitely if no constraining force is applied in the wall-parallel direction. To prevent this, the velocity of those particles for which δ_s is smaller than the particle radius is adapted such that it relaxes toward the no-slip boundary condition with a characteristic time scale t_{relax} . This relaxation is achieved by the introduction of an additional force $\mathbf{F}_{\text{relax}}^{\text{wall}}$ that has the form

$$\mathbf{F}_{\text{relax}}^{\text{wall}} = \Psi_p \xi \mathbf{F}_{\text{relax}} \quad (10)$$

where Ψ_p is a coefficient vector that scales with the expected velocity deviation of the primary particle after t_{relax} if $\mathbf{F}_{\text{relax}}^{\text{wall}}$ would not be applied. The unknown scalar variable F_{relax} in eq 10 is the same for all primary particles in the agglomerate; it is found by minimizing the root-mean-square velocity deviation of the deposited particles after t_{relax} . In the case that the magnitude of either the wall-normal or wall-parallel component of the total particle–wall interaction force, given by $\mathbf{F}_{\text{s-d}} + \mathbf{F}_{\text{relax}}^{\text{wall}}$ for any primary particle exceeds the maximum magnitude (which is equal to γF_L^N in the wall-normal direction and γF_L^S in the wall-parallel direction), this component is truncated and the minimization process is repeated until a consistent set of values for $\mathbf{F}_{\text{relax}}^{\text{wall}}$ is obtained for all particles.

■ SELECTION OF CASES

Continuous-Fluid Flow. All parameters of the continuous-flow solver are non-dimensionalized by the channel height H , fluid viscosity η_f and density ρ_f and pressure-gradient velocity u_∇ . As a result, a single-phase fluid flow can be fully described by the pressure-gradient Reynolds number Re_∇ , defined by

$$Re_\nabla = \frac{\rho_f u_\nabla H}{\eta_f} \quad (11)$$

where u_∇ is defined as

$$u_\nabla = \sqrt{-\frac{1}{2} \frac{\partial p}{\partial x} \frac{H}{\rho_f}} \quad (12)$$

where $\partial p/\partial x$ is the pressure gradient that is the driving force of the flow. In this work, we consider turbulent channel flows with Re_∇ ranging from 360 to 1080, corresponding to bulk Reynolds numbers between 5700 and 19 400. DNS are used at modest Reynolds numbers, whereas LES are used at elevated Reynolds numbers, where DNS become computationally very expensive. For the fluid flow, periodic boundary conditions are used in the streamwise (x) and spanwise (y) directions and a no-slip boundary condition is used at the faces of the channel walls that are located at $z = 0.0$ and 1.0 . A uniform grid is used in the x and y directions. In the z direction, the resolution is higher near the walls than in the center of the channel. The turbulent flow is statistically steady before the dispersed phase is introduced. The parameters associated with the continuous liquid carrier phase are given in Table 1.

Table 1. Overview of Parameters Associated with the Continuous Liquid Carrier Flow^a

Re_∇	360	540	720	1080
Re_{bulk}	5700	9000	12 500	19 400
$(n_x, n_y, n_z) = (96, 64, 48)$	LES			
$(n_x, n_y, n_z) = (192, 128, 96)$	DNS	LES	LES	LES
$(n_x, n_y, n_z) = (320, 224, 160)$				DNS
L_x, L_y, H			5, 2, 1	

^a L_x, L_y and H denote the dimensions of the computational domain in the streamwise, spanwise, and wall-normal directions (the same in all simulations); the number of grid nodes in these directions is given by n_x, n_y and n_z , respectively.

Dispersed-Phase Parameters. The results presented in this work can be separated into two distinctive parts. First, we study the transport, agglomeration, and breakup of particles under turbulent flow conditions, in the absence of deposition and re-entrainment. Next, we consider deposition and re-entrainment of agglomerates at the walls of the flow domain, comparing the results for different parameters of the deposition model. In both cases, primary particles are introduced in the computational domain by inserting them at uniformly distributed random locations, while preventing overlap with the other particles that are already present in the domain. Upon injection, the velocity of the particles is set equal to the local velocity of the continuous fluid phase.

Apart from the parameters of the deposition model, which will be discussed later, the dispersed-phase parameters are given by the radius of the primary particles (R_p), the volume fraction (ϕ_p) and number of primary particles, the added-mass corrected particle–fluid density ratio ($\check{\rho}_p/\rho_f$), and the maximum stresses that the interparticle bonds can withstand before breaking (F_L^N, F_L^S, T_L^B , and T_L^T). In this work, we consider particles that are monodispersed, with a radius equal to 0.5% of the channel height H . This relatively large primary particle size is adopted because it results in sufficiently large collision rates at moderate primary particle numbers, allowing for simulations to achieve steady state in a tractable amount of simulation time. Since typical asphaltene densities are about 1200 kg/m³,²² and for light crude oils, oil densities can be as low as 800 kg/m³, the density ratio ρ_p/ρ_f is set equal to 1.5 throughout this work. This gives an effective density ratio $\check{\rho}_p/\rho_f$ equal to 2.0.

The maximum stresses that the interparticle bonds can withstand before breaking are the main parameters of interest in this work. For interpreting the results, F_L and T_L are scaled by the characteristic non-dimensional hydrodynamic force and torque acting on a single primary particle in a turbulent flow, which can be obtained by non-dimensionalizing eq 2 using the channel height H , the pressure-gradient velocity u_∇ , and the fluid density and viscosity ρ_f and η_f . The rescaled parameters can be expressed as

$$F_L^* = \frac{F_L Re_\nabla H}{6\pi R_p}; \quad T_L^* = \frac{T_L Re_\nabla H^2}{6\pi R_p^2} \quad (13)$$

Multiple values of F_L^* and T_L^* are considered; their values are chosen such that the number of primary particles per agglomerate in steady state is of $O(100)$. Agglomeration numbers of this order were selected such that, on the one hand, a significant number of agglomerates can be simulated with a tractable number of primary particles yet, on the other hand, it remains feasible to attribute macroscopic properties (e.g., shape, fractal dimension, etc.) to the agglomerates.

Steady State of Agglomeration and Breakup. In the simulations of agglomeration and breakup in the absence of deposition and re-entrainment, phase separation is considered to have occurred before the start of the simulations, such that the volume fraction and the number of primary particles are constant in time. We use a fixed number of particles equal to 250 000 for these simulations, corresponding to $\phi_p = 1.3\%$. Spatially, the primary particles are random-uniformly distributed over the entire computational domain upon initialization. The dimensions of the computational domain are

equal for the particles and the continuous phase, and periodic boundary conditions are used for the particles in the streamwise and spanwise directions, like they are for the fluid. Agglomerates are considered to be broken by only one breakup mechanism per case considered. The range of interparticle bond strengths studied is given by $F_L^* = [19.7, 157.2]$ and $T_L^* = [172, 3092]$. This corresponds to the bonds being able to withstand stresses that are significantly larger than those induced by the flow on a single primary particle.

Deposition and Re-entrainment. As an example case for real asphaltene deposition, we consider the formation of a deposit layer from primary particles that are released at a continuous rate in a designated phase-separation region, located in the upstream part of the flow domain, between $x = 0.0$ and 2.5 . Periodic boundary conditions for the dispersed phase are only used in the spanwise direction in these simulations; in the streamwise direction, the domain length for the particles is equal to 11 times the continuous-phase domain length (SSH), preserving the periodic boundary conditions for the fluid phase. At the downstream end of the domain, an outflow boundary condition for the dispersed phase is considered, by removing agglomerates once their first primary particles reach $x = 55$. To remove the effects of this boundary conditions from the simulation results, the deposit layer properties are only studied in the region between $x = 0.0$ and 50 . We consider phase separation to occur for a given time interval and study the characteristics of the deposit layer after the phase separation has taken place. No particles are present in the domain upon the initialization of simulations, and particles are injected at a continuous rate per unit volume of the phase-separation region and per unit of time (N_p), between $t = 0.0$ and 5.0 , after which the injection of particles is stopped and the deposit layer is allowed to settle until $t = 10.0$, before studying its properties. In all deposition cases, one-way coupling is applied and particles are considered to be broken by all four breakup mechanisms simultaneously. The presented results are averaged over five simulation runs, with different initial conditions, to improve statistical accuracy.

The model parameters that have been considered for the deposition study are summarized in Table 2. The values of γ are chosen such that

Table 2. Overview of Model Parameters Considered in Particle Deposition Simulations

parameter	reduced	base	increased
F_L^*	39.3	78.6	157.2
T_L^*	515	1546	4639
γ		0.1	0.3, 0.75
R_c	2.5×10^{-2}	5.0×10^{-2}	
t_{relax}		2.5×10^{-4}	1.0×10^{-3}
ζ	0.5	1.0	2.0
N_p		10 000	20 000

the interaction force between the particles and the wall is smaller than between particles mutually, whereas R_c is chosen larger than the particle diameter to ensure that a significant amount of particles is attracted to the walls. The base value of t_{relax} is approximately equal to the time step taken by the continuous- and dispersed-phase solvers; no reduced value is studied for this parameter, because this would cause instability (since we consider the agglomerate acceleration to be constant throughout the time step, overshoots would occur). The different values of ζ that are used correspond to the spring-dashpot system to be underdamped, critically damped, and overdamped, respectively. The values of N_p are chosen such that, in total, 250 000 and 500 000 particles are injected per simulation, keeping the number of primary particles tractable.

RESULTS AND DISCUSSION

Transport, Agglomeration, and Breakup. In the absence of deposition and re-entrainment, the balance between agglomeration and breakup (which are competing processes) gives rise to a dynamical steady state, in which individual

agglomerates constantly undergo collision and breakup events and, thus, change over time. We study here how the properties of the steady-state agglomerate population depend upon the model parameters and simulation mode employed. The properties that are presented here are the shape distribution, the fractal dimension, and the mean mass of the agglomerate population. The results presented are obtained by interpreting various uncorrelated steady-state agglomerate snapshots to gain sufficient statistical data.

Agglomerate Shape. To study to what extent the shape of the agglomerates formed is affected by the mechanism of agglomerate breakup, the characteristic strength of the interparticle bonds, and the properties of the continuous fluid phase, we present here results on the cumulative agglomerate shape distribution function, that represents the probability that a randomly selected agglomerate has a certain shape. To this end, each agglomerate is represented by an ellipsoid (the length of the axes of the ellipsoid are equal to the length of the agglomerate along each of its primary axes of inertia). The ratios of the axes of this ellipsoidal representation can then be used to characterize the shape of the agglomerates. Figure 2 shows the average cumulative agglomerate shape distribution functions for the different breakup mechanisms considered in this work, along with examples of agglomerates that are representative of certain regions of this distribution function.

It is found that the shape of the agglomerates is hardly sensitive to the breakup mechanism considered. The most probable agglomerate shape has proportions of approximately 1.4/1.0/0.7 for the major, intermediate, and minor axes (inverting the ratio between the latter two), respectively, corresponding to slightly flattened and elongated sphere-like shapes. In Figure 3, the influence of DNS versus LES, one- and two-way coupling, and the strength of the interparticle bonds on the agglomerate shape are shown, for the straining and shearing breakup mechanisms. From these results, it can clearly be inferred that the shape of the agglomerates formed is similar when one- and two-way coupling are considered, as well as for both DNS and LES; likewise, it is found that the Reynolds number has a negligible influence on the agglomerate shape. The same observations hold true for breakup by bending and twisting (shown in the Supporting Information). Furthermore, only a slight dependence of the agglomerate shape upon the strength of the interparticle bonds is found: for increasingly strong agglomerates, the shape distribution functions shift slightly toward lower values of the axes ratios (viz., the agglomerates become slightly more spherical). This effect is most pronounced for the shearing breakup mechanism, while it is least for straining; the dependences for bending and twisting lay somewhere midway between these extremes.

Fractal Dimension. Fractal dimensions describe how certain properties (such as the surface area or the mass) scale with the linear dimensions of self-similar objects. Here, we study how the mass-fractal dimension of the steady-state agglomerate population varies with the model parameters and breakup mechanisms. To this end, D_f is defined such that

$$\check{m}_a \propto R_g^{D_f} \quad (14)$$

where \check{m}_a represents the agglomerate mass and R_g is a representative radius of the agglomerates. In this work, we use the radius of gyration for representing the agglomerate radius, which is defined as

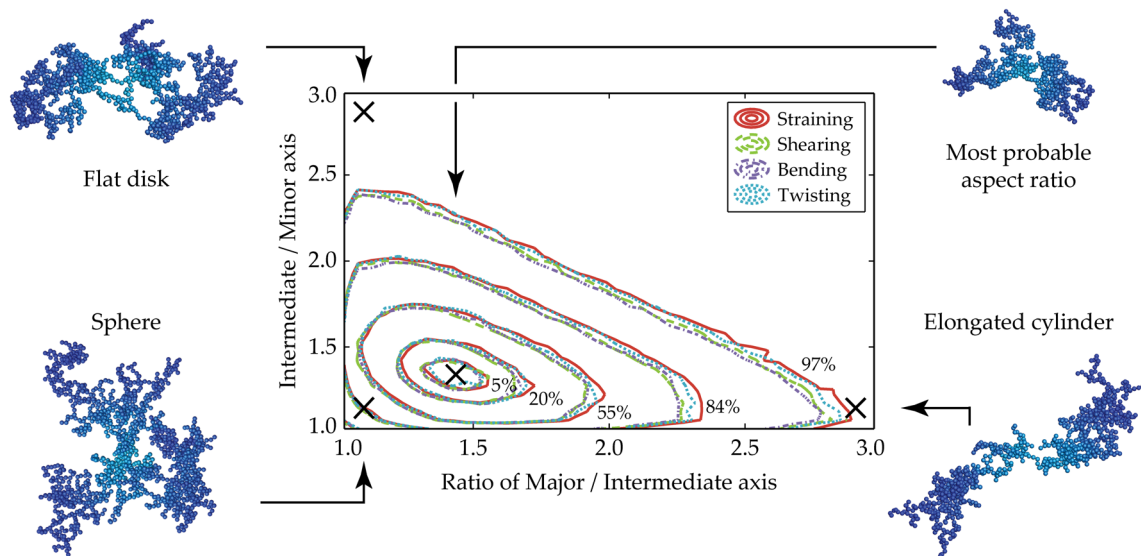


Figure 2. Steady-state cumulative agglomerate shape distribution functions averaged over all model parameters considered per breakup mechanism. The numbers indicated by the contours denote the percentage of the total agglomerate population that has a form factor contained within those contours (viz., the probability that an agglomerate picked at random has a particular form factor). The sample agglomerates shown provide a visual indication of representative agglomerate shapes for different regions of the distribution function.

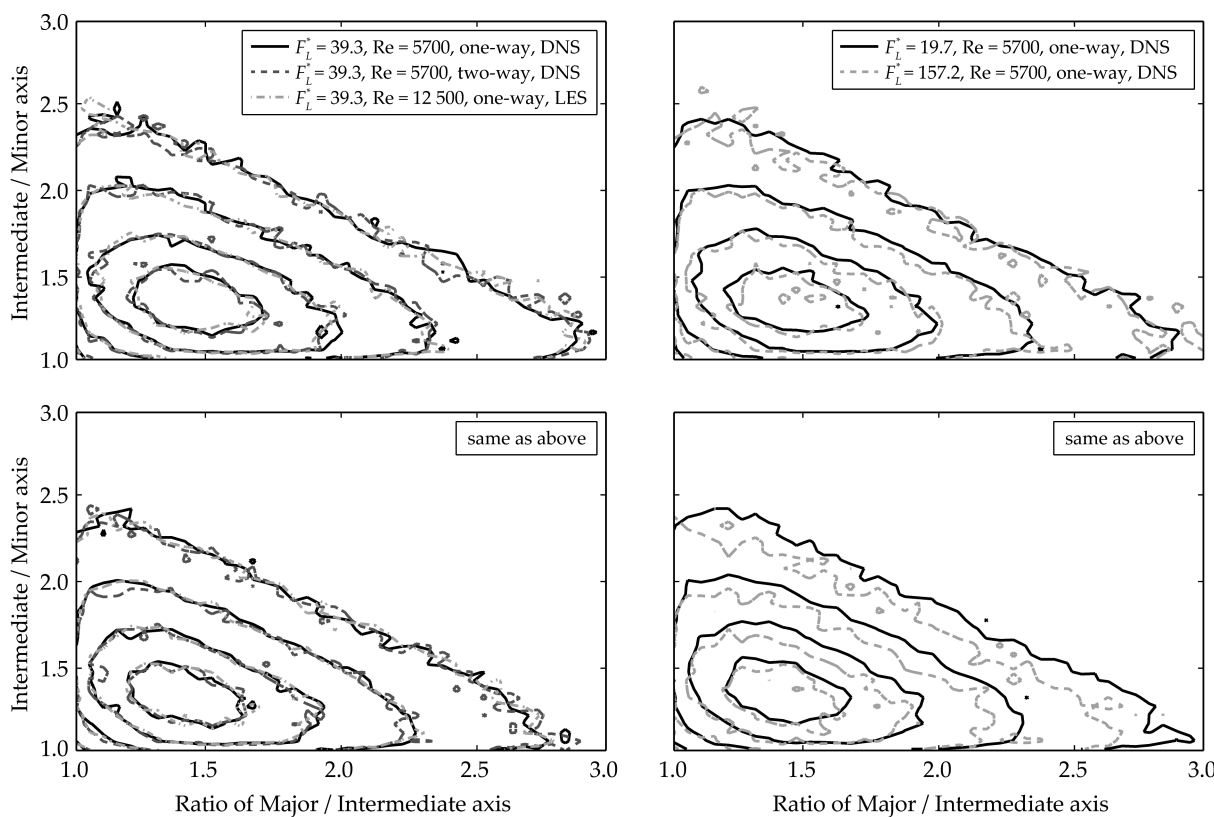


Figure 3. Steady-state cumulative agglomerate shape distribution functions for different simulation modes, one- and two-way coupling, Reynolds numbers, and F_L^* , for agglomerates that are broken by straining (top) and shearing (bottom). The contour levels are the same as in Figure 2; the 5% contour has been omitted to improve level distinguishability.

$$R_g \equiv \sqrt{\frac{1}{n} \sum (\mathbf{r}_p \cdot \mathbf{r}_p)} \quad (15)$$

where the sum runs over all primary particles in the agglomerate. To determine the fractal dimension of the agglomerates, expression 14 is fit to a large ensemble of

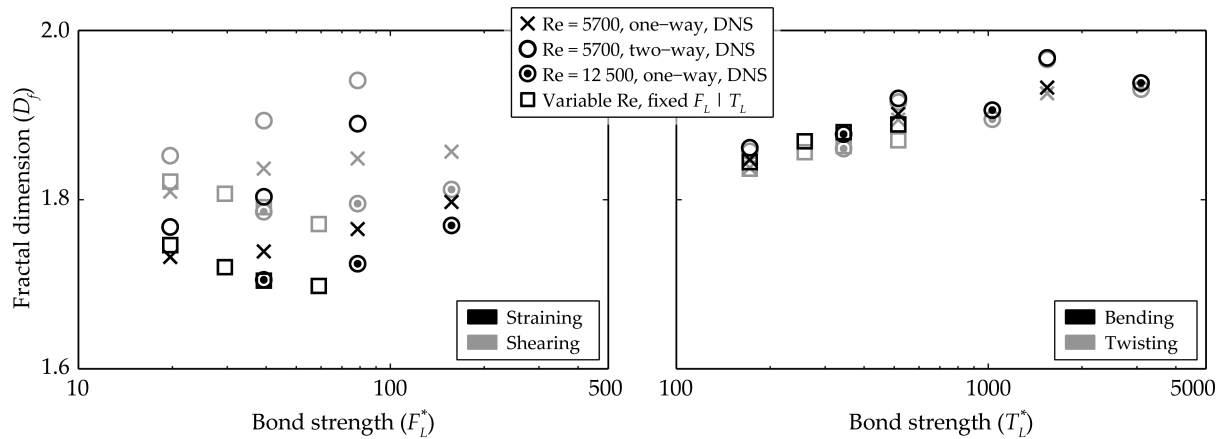


Figure 4. Fractal dimensions for steady-state agglomerate populations broken by straining and shearing (left) and bending and twisting (right). The simulations with variable Reynolds numbers are one-way coupled LES simulations, in which the values of F_L and T_L have been fixed at 5.15×10^{-3} and 2.25×10^{-4} , respectively, and the Reynolds number is varied between 5700 and 19 400 to arrive at varying values of F_L^* and T_L^* .

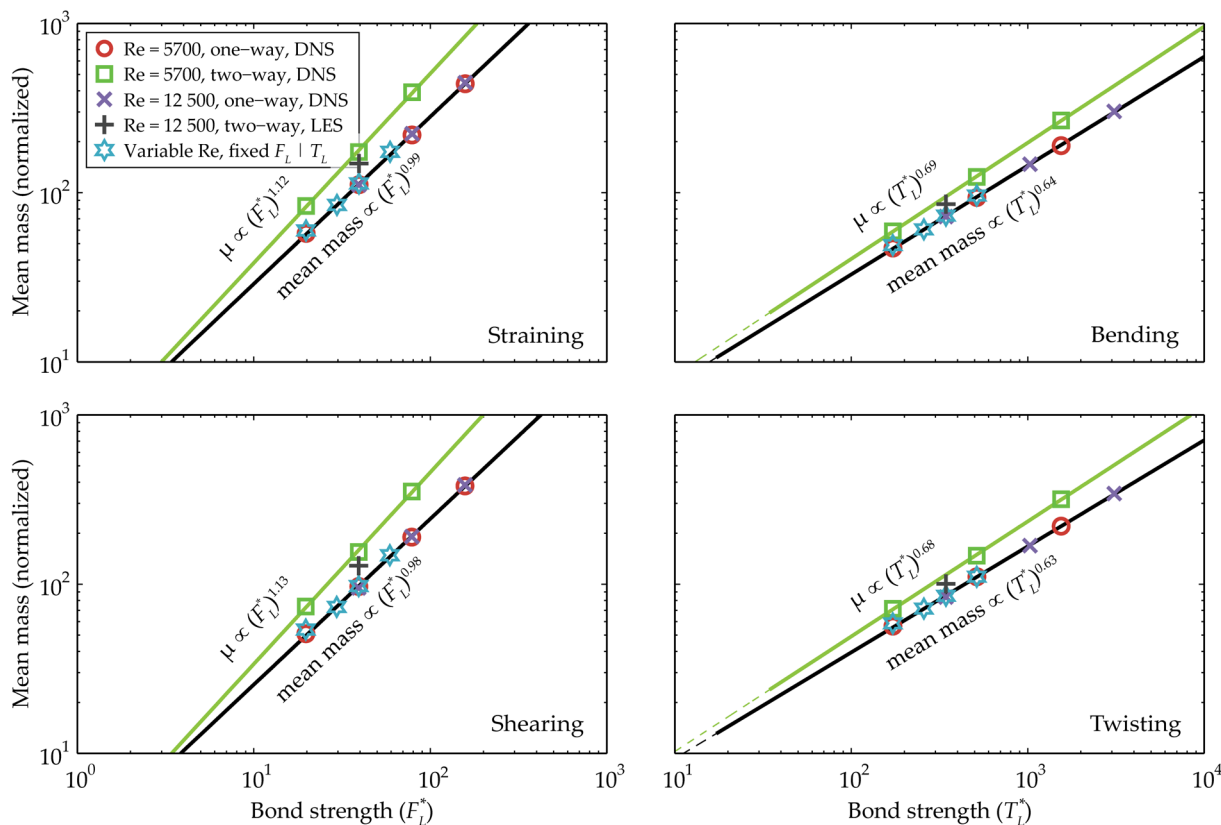


Figure 5. Scaling of the mean agglomerate mass with the characteristic strength of the interparticle bonds, for different breakup mechanisms, one- and two-way coupling, and multiple Reynolds numbers; the legend shown applies to all graphs. The simulations with variable Reynolds numbers are one-way coupled LES simulations, with the same configuration as described in the caption of Figure 4.

(\check{m}_v , R_g) data points, obtained from steady-state agglomerate populations. Figure 4 summarizes the results obtained this way. In general, it is found that the fractal dimension of the agglomerates monotonically increases with increasing values of F_L^* and T_L^* , indicating a slight restructuring to a more compact morphology. Two-way coupling promotes larger values of D_f than one-way coupling; this effect is stronger for the force-induced breakup mechanisms than for the torque-induced

mechanisms and becomes more pronounced at elevated values of F_L^* and T_L^* . While the fractal dimensions increase with increasing values of both F_L^* or T_L^* and D_f is smallest for the one-way coupled force-induced breakup mechanisms, intermediate for the torque-induced breakup mechanisms (independent of whether one- or two-way coupling is used), and largest for the two-way coupled force-induced breakup mechanisms.

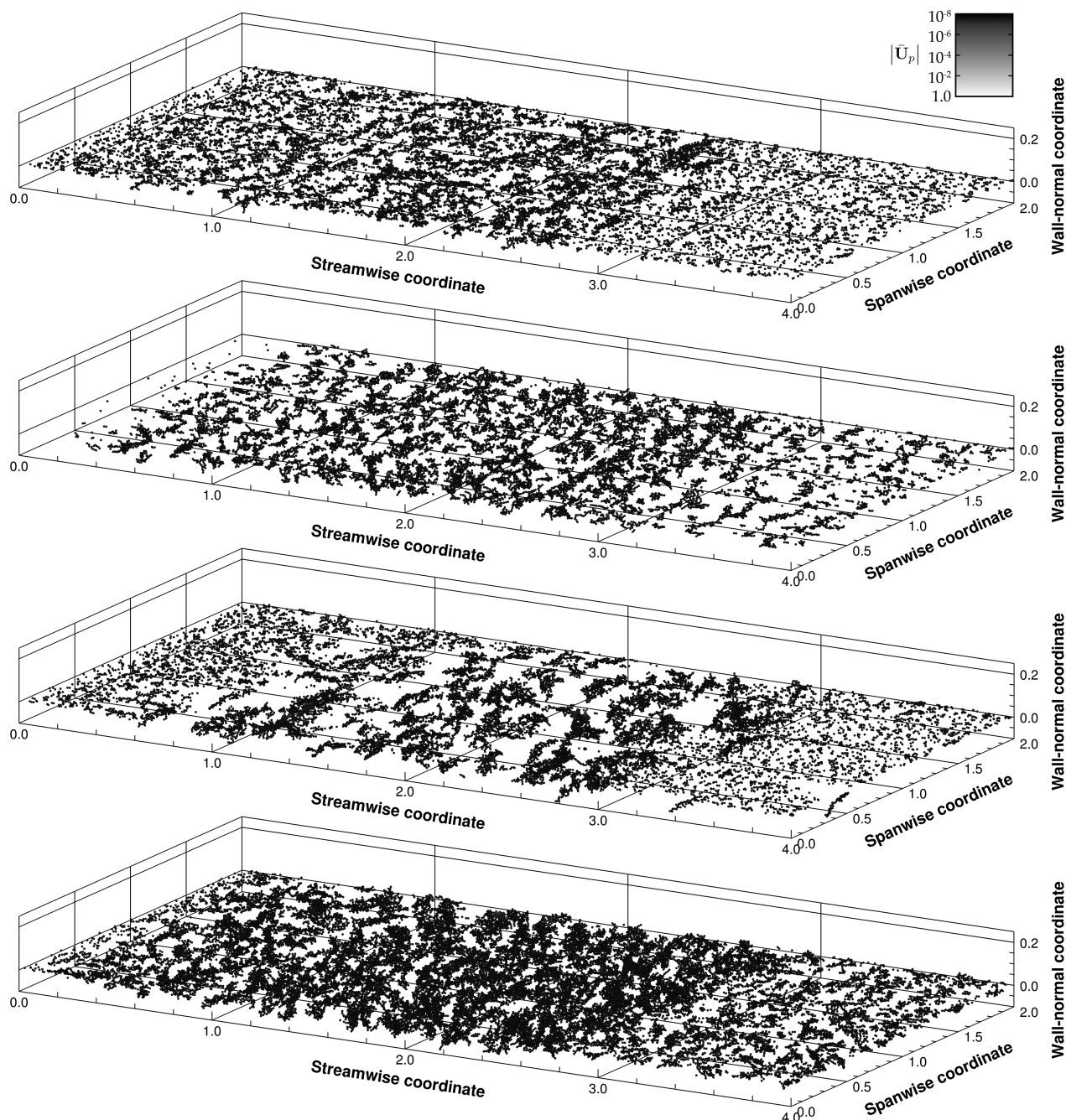


Figure 6. Examples of deposit layers formed under various model conditions; snapshots are taken at $t = 10.0$. From top to bottom: base case, reduced F_L^* and T_L^* , $t_{\text{relax}} = 1.0 \times 10^{-3}$, and $N_p = 20\,000$.

For the lowest values of F_L^* and T_L^* considered, the results of the one-way coupled DNS and LES simulations are both obtained at a bulk Reynolds number equal to 5700. The results shown in Figure 4 thus reveal that the fractal dimension is hardly sensitive to the applied simulation mode. Since the Reynolds number increases for increasing values of F_L^* and T_L^* in the LES simulations, we find that the fractal dimensions of the agglomerates decrease with increasing values of the Reynolds number. This finding is confirmed by a direct comparison of the DNS results obtained at $Re = 5700$ and 12 500. Overall, the values of D_f found in this work compare favorably to experimentally observed asphaltene fractal

dimensions reported in the literature.²³ With confirmation of visual observations, such as the sample agglomerates shown in Figure 2, the range of fractal dimensions obtained indicates that the agglomerates have a very open, porous structure.

Scaling of Mean Mass. As a last property of the steady-state agglomerate populations, we study how the mean mass of the agglomerates scales with the characteristic strength of the interparticle bonds, for the different breakup mechanisms considered, one- and two-way coupling, and multiple Reynolds numbers. The results are summarized in Figure 5.

Focusing first on one-way coupling and looking at the linear breakup mechanisms (viz., straining and shearing), it is found

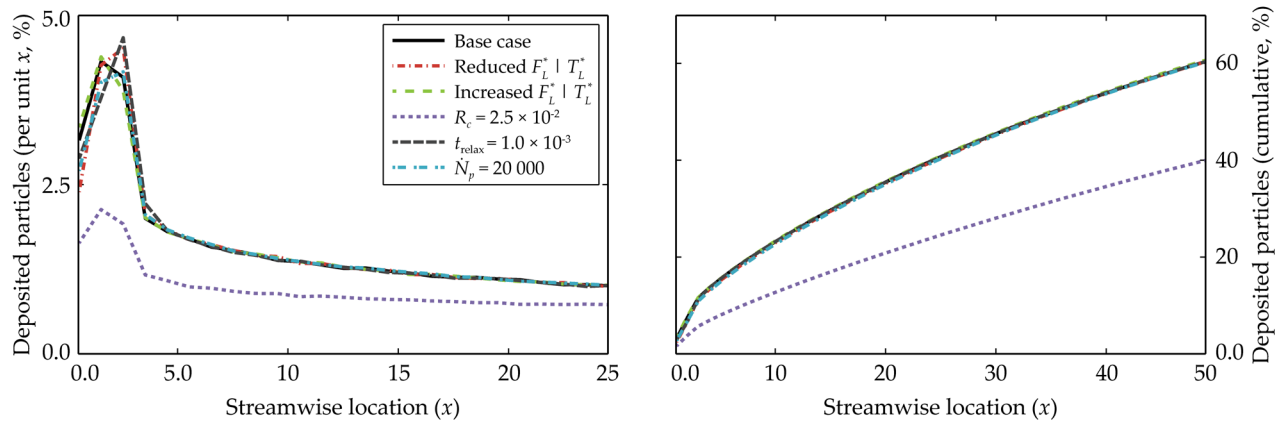


Figure 7. Percentage of injected particles that have deposited per unit of channel length (left) and cumulative percentage of deposited particles (right) as a function of the streamwise coordinate; the legend applies to both graphs. The results for $\gamma = 0.3$ and 0.75 , and for $\zeta = 0.5$ and 2.0 (shown in the Supporting Information) feature profiles that are very similar to those of the base case.

that the mean mass of the agglomerates scales linearly with the strength of the interparticle bonds; results obtained at different Reynolds numbers follow the same scaling relations, for both the DNS and the LES simulations. For the bending and twisting breakup mechanisms, the mean mass of the agglomerates scales with the characteristic bond strength to an approximate two-thirds power; for these mechanisms, the one-way coupled results obtained at different Reynolds numbers using both DNS and LES also favorably agree with common scaling relations. The decrease of the scaling exponents with respect to the linear breakup mechanisms can be explained by the fact that the induced torque scales with the product of the linear dimension of the agglomerate and the induced force. Considering a typical value of the fractal dimension to be 1.9, the radius of the agglomerates scales to the mean mass roughly by a $1/1.9$ power. Since we find that the induced forces scale linearly with the mean mass of the agglomerates, a simple analysis yields that the mean mass will approximately scale with the torque to the $1 + 1/1.9$ power. When inverted, this corresponds favorably to observed scaling exponents of the mean mass with respect to the induced torque (because the inverse of $1 + 1/1.9$ is equal to 0.66).

When considering two-way coupling and DNS at a Reynolds number of 5700, the scaling exponents relating the mean agglomerate mass to the strength of the interparticle bonds increase somewhat with respect to the one-way coupled values for all the breakup mechanisms. Furthermore, the agglomerates grow to larger masses in all cases when two-way coupling is considered instead of one-way coupling, indicating that agglomerate breakup becomes relatively less effective with respect to agglomeration if the effect of the dispersed phase on the fluid-phase momentum equations is taken into account. Looking at the single two-way coupled data points that have been obtained for each breakup mechanism at the elevated Reynolds number of 12 500, it is observed that, in contrast to the one-way coupled simulations, these results do not coincide with the two-way coupled scaling relations obtained for $Re = 5700$ but, consistently, fall below them for all breakup mechanisms. This suggests that the Reynolds number independence of the scaling relations for the mean agglomerate mass found in one-way coupling no longer holds true when

two-way coupling is considered; further research is required to elucidate this finding.

We have verified, however, that, for both one- and two-way coupling, the scaling relations obtained for the mean mass in the turbulent flow regime do not hold true in laminar flow. In one-way coupled laminar-flow simulations, the streamwise fluid velocity profile is purely parabolic. Due to the lack of spanwise and wall-normal velocity components, agglomerates will grow to practically infinite size, as confirmed by our simulations. In two-way coupling, the presence of the agglomerates changes the parabolic velocity profile of the flow, and therefore, the situation becomes more complex. Currently, we are investigating this situation in more detail, considering both laminar flows as well as flows with Reynolds numbers that are transitional between the laminar and turbulent flow regimes.

Deposition and Re-entrainment. To monitor the performance of the deposition model and to check its sensitivity with respect to the model parameters, we present here results on the total amount and the spatial distribution of deposition, as well as on the properties of the agglomerates that constitute the deposit layer. Figure 6 shows examples of deposit layers formed under several model conditions.

Time-Step Constraints. Although completely unaffected by most of the parameters of the deposition model, the time-step constraint imposed by the particulate phase was found to vary with the particle–wall interaction coefficient γ . At values of γ equal to 0.3 and 0.75, a decrease in the time step of 5 and 37% with respect to the base case ($\gamma = 0.1$) was found, respectively. This time-step reduction is caused by an increase of the wall-normal velocity component of particles as they are attracted toward the wall, due to the increased magnitude of the attractive particle–wall interaction force, given by expression 7.

Amount of Deposition and Spatial Distribution. In Figure 7, the number of deposited particles is expressed as a percentage of the total number of injected primary particles, both per unit of domain length as well as cumulative from $x = 0.0$ onward, for several of the cases considered in this work. In general, we find that the total fraction of the injected particles that deposits somewhere inside the domain depends only upon the wall-adhesion interaction range R_c . Because R_c affects the extent of the region near the channel walls in which particles experience attractive forces toward the wall, this result indicates

that not the adhesion properties but rather the supply of primary particles toward the walls is the limiting factor for deposition under the conditions considered. This finding is confirmed by the fact that, for the doubled particle injection rate, $\dot{N}_p = 20\,000$, the spatial deposition profile is almost the same as for the base injection rate, such that twice as many particles deposit on the walls when the supply of particles is increased twofold.

As particles are released in the computational domain between $x = 0.0$ and 2.5 , the results in Figure 7 show that deposition predominantly takes place in a region close to the location where the separation of primary particles takes place. The spatial profile of deposition is similar for different model conditions; the only real exception to this is the increased value of the wall-adhesion relaxation time t_{relax} for which a pronounced shift in the downstream direction is observed for the peak of the deposition profile inside the phase-separation zone compared to the other cases considered. This effect can be attributed to the fact that, for larger values of t_{relax} the streamwise velocity of deposited particles takes longer to relax to zero, thereby allowing the particles to creep further downstream over the walls during deposition or after receiving momentum when other particles or agglomerates impact them.

Properties of Agglomerates in the Deposit Layer. Even though we find that the spatial distribution of deposited primary particles is to a large extent independent of the model parameters considered, this does not necessarily imply that all properties of the deposit layer are unaffected (as is also clear from the visual deposit layer examples shown in Figure 6). To study the morphology of the deposit layer in more detail, we consider here how the agglomeration number of the deposited agglomerates (as measured by the number of constituent primary particles, $N_{p/a}$), the thickness of the deposit layer and the area fraction of the walls that is covered by particles depend upon the values of F_L^* and T_L^* , γ , R_c , t_{relax} , ζ , and \dot{N}_p . These results are summarized in Figure 8.

Considering the results presented in Figure 8, combined with visual inspections of the deposit formation process, we propose that the trends found in the properties of the deposit layer can to a large extent be attributed to two features: first, the local concentration of deposited primary particles and, second, the mobility of the deposited agglomerates (viz., to what extent they can move with respect to the walls). As a measure for the particle mobility, the mean absolute velocity of the deposited primary particles ($|\bar{U}_p|$) at $t = 5.0$ is shown at the top of Figure 8 for the different downstream regions that are considered. When the results obtained for different cases are compared to the base-case results, it is found that, first, the mobility of the deposited agglomerates is inversely proportional to the value of γ . This can be explained by the fact that an increasing strength of the forces exerted by the walls on the particles will cause the particles to adapt quicker to the stationary walls, thereby lowering their average velocity. For the same reason, the mobility is inversely proportional to changes in F_L^* and T_L^* , as the wall-interaction forces scale with F_L^* . Increasing the value of the damping factor ζ or the parameter t_{relax} is found to increase particle mobility.

To demonstrate that the morphology of the deposit layer mainly depends upon $|\bar{U}_p|$ and the local concentration of deposited primary particles, the bar graphs shown in Figure 8 have been sorted in ascending order of the particle mobility and cases for which the number density of deposited particles deviate significantly from the base case have been hatched.

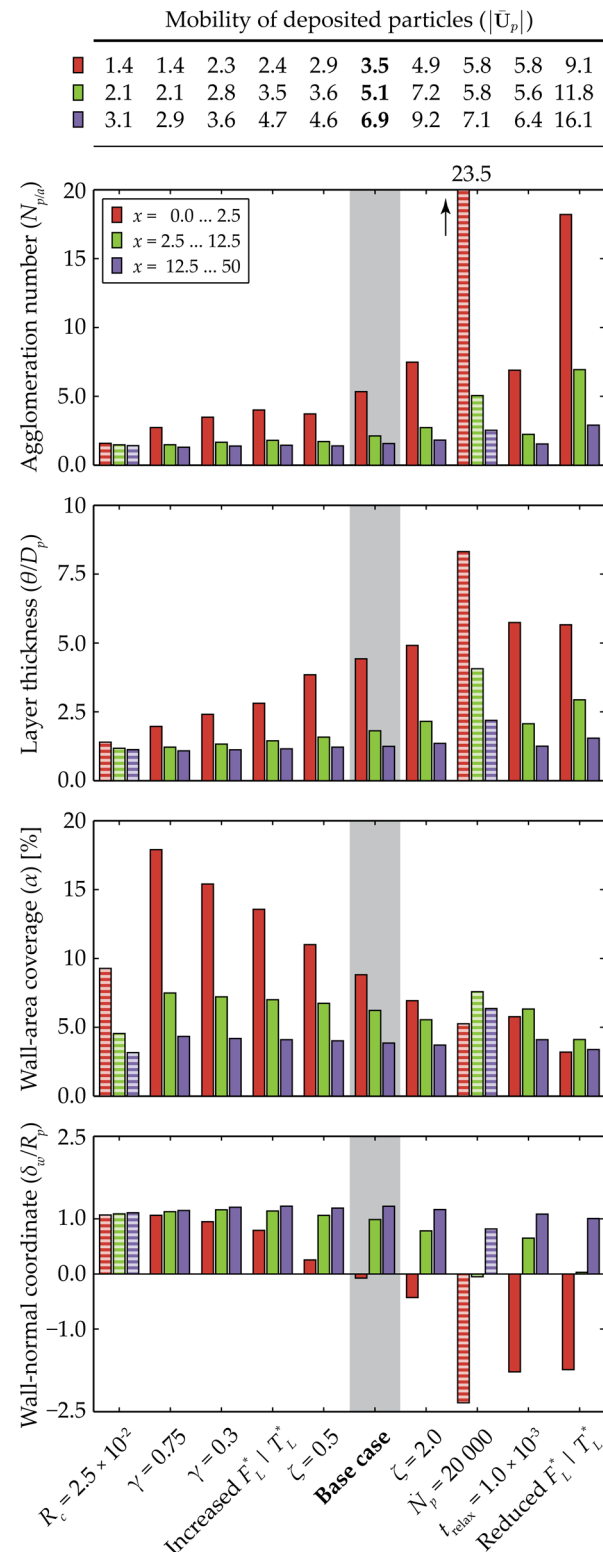


Figure 8. Characteristics of the deposit layer morphology at $t = 10.0$. From left to right, bars are sorted by ascending values of $|\bar{U}_p|$ for $x = 0.0 \dots 2.5$ (the phase separation region). The values of $|\bar{U}_p|$ are obtained at $t = 5.0$ and are multiplied by 100 for legibility. Hatched bars indicate cases in which the total number of deposited particles deviates significantly from the base case.

The top graph of Figure 8 shows an overview of the average number of primary particles that constitute one deposited

agglomerate ($N_{p/a}$), as a function of the streamwise coordinate, for all cases considered in this work. The trends found for $N_{p/a}$ can be explained by the fact that the number of primary particles per deposited agglomerate is strongly dependent upon the propensity of deposited agglomerates to collide into each other. This likelihood scales with the mobility of the deposit layer, because this determines the wall area that agglomerates can sample per deposition event; it also scales with the number of deposited particles that are present in this area. As such, the $N_{p/a}$ remains low in the downstream region of the computational domain (viz., far from the region where primary particles are injected), because the number density of deposited particles per unit area is low in this range, preventing deposited particles from touching each other, even if some of them temporarily gain momentum after being hit by newly depositing particles. Inside the phase-separation zone, however, the variation in deposition concentration and particle mobility has a large impact on the number of primary particles per agglomerate, and a trend of increasing $N_{p/a}$ with increasing $|\bar{U}_p|$ is observed. In combination with the fact that the concentration of deposited particles increases with increasing values of \dot{N}_p and decreases with R_c , as was shown earlier, these observations support the conclusion that the particle mobility and deposit concentration can explain the trends in $N_{p/a}$ found in Figure 8.

Next, we study the thickness θ of the deposit layer, also shown in Figure 8 (normalized by the primary particle diameter $D_p = 2R_p$). The thickness is determined by dividing the walls of the computational domain into square patches, with edge lengths equal to 10 times the primary particle diameter and, subsequently, determining the minimum and maximum wall-normal coordinate for all particles that have their center falling in this patch. The outer and inner coordinates of the deposit layer are then averaged over the isotropic spanwise direction and subtracted from each other. The increase and decrease of the deposit layer thickness with different model parameters can be explained by a close relation to the number of primary particles per agglomerate and, thus, shows trends similar to those found for $N_{p/a}$. For low values of $N_{p/a}$, doublets and triplets to a large extent are the largest agglomerates formed; these tend to lay flat on the wall, corresponding to a deposit layer thickness that is equal to just one particle diameter. For high values of $N_{p/a}$, in contrast, the deposited agglomerates tend not to form sheet-like structures that can lay flat on the wall but rather take on a three-dimensional shape similar to the sample agglomerates shown in Figure 2. As a result, their primary particles will protrude inside the flow domain and into the walls, thereby resulting in a thicker deposit layer.

As a measure of the area fraction α of the walls that is covered by deposited particles, we compute the intersected area of all primary particles that are part of the deposit layer with a plane parallel to the walls of the flow domain, located one particle radius inside of it; the results obtained this way are also shown in Figure 8. Like for the deposit layer thickness, the three-dimensional morphology of the deposited agglomerates for high values of $N_{p/a}$ explains the variations of the wall coverage in the region with the lowest x coordinates. This is because, at a constant concentration of deposited particles, a thicker three-dimensional deposit layer corresponds to decreasing values of the intersected area of a particular plane near the wall. Consequently, the wall-area coverage decreases with increasing values of $|\bar{U}_p|$. When the value of $N_{p/a}$ is low, however, in the downstream region of the flow domain, where the deposited agglomerates are predominantly aligned with the

walls, the covered wall area only varies significantly with the amount of deposition, that is, with \dot{N}_p and R_c .

Because, from the perspective of the deposition, the walls of the flow domain are modeled as soft entities, which do not force particles to stop moving completely upon reaching the coordinate of the walls, a significant amount of particles may protrude through the walls, to finally end up at locations outside of the actual flow domain (note that, for such particles, the hydrodynamic force is calculated by assuming that the fluid velocity is zero). The last graph in Figure 8 shows the average wall-normal coordinate of the deposited primary particles, δ_w , normalized by the primary particle radius R_p . For all model conditions, the particles nicely reside on the face of the walls in the region where the deposit layer consists of small agglomerates (as indicated by the non-dimensional coordinate of around 1). Especially toward the upstream end of the domain, the particles can significantly penetrate the walls, increasing in severity with increasing deposit layer thickness, agglomeration number, and, thus, also with increasing deposit mobility. This issue will have to be addressed further in future developments of the model, for instance, by increasing the relative strength of the repulsive part of the wall-adhesive potential with respect to the attractive part.

CONCLUSION

To obtain a better fundamental understanding on the agglomeration and deposition of asphaltenes under flow conditions, in this work, an advanced numerical model for asphaltene agglomeration and deposition is proposed, as induced by a turbulent liquid carrier phase, in which transport, breakup, and re-entrainment are also taken into account. All four principal mechanisms of breakup (straining, shearing, bending, and twisting) are included in this model, and the internal structure of the agglomerates is tracked in time. A novel treatment for adhesive wall boundary conditions in the context of structure-resolved Lagrangian agglomerate tracking is proposed, in which the attractive particle–wall interaction is modeled using a damped harmonic oscillator, combined with a time relaxation to enforce no-slip boundary conditions for the deposited particles. Ultimately, the performance of the model should be evaluated against measurements of actual asphaltene deposition (as will occur either in the laboratory, or during field operations), but that is a subject for future work.

The results of our simulations show that, from a pragmatic perspective, the properties of the steady-state agglomerate population formed in the absence of deposition and re-entrainment are invariant to whether DNS or LES simulations are conducted; this suggests that the latter, less computationally intensive method can be used for future studies. In contrast, it is found that the characteristics of the agglomerates change when, instead of one-way coupling (in which the forces exerted by the particles on the fluid are neglected), two-way coupling is applied, underlining the necessity to include the particle–fluid interactions in the simulations.

We have demonstrated that the shape of the agglomerates is to a large extent universal with respect to the mechanism by which the agglomerates are broken, as well as to the characteristic strength of the bonds between the primary particles. Agglomerates have a very open structure, as is confirmed by the range of fractal dimensions found, which corresponds favorably to values reported earlier in the literature for asphaltene agglomerates; they become slightly more compact when their strength is increased. In the one-way

coupled turbulent flow regime, the mean mass of the agglomerates is well-predicted by scaling relations that are independent of the Reynolds number; further research is required to elucidate to what extent similarly general scaling relations for two-way coupled systems can be obtained. In general, our results show that the properties of the agglomerates for different combinations of model parameters can be readily predicted from the results of a limited set of simulations.

As an example case for real asphaltene deposition, the formation of a deposit layer from primary particles that are released at a continuous rate in an upstream region of the flow domain is considered in this work. It is found that, for the cases considered, the spatial distribution and the total amount of deposition is limited by the supply of primary particles toward the walls of the flow domain rather than the adhesion parameters of the deposition model, showing that, from this perspective, the model is insensitive to most of its parameters. Deposition predominantly takes place in a region close to where particles are injected; the amount of deposition rapidly decreases for larger streamwise coordinates. On the other hand, the morphology of the deposit layer varies significantly with the parameters of the deposition model. The observed trends in the agglomeration number, thickness, wall-area coverage, and average wall-normal coordinate of the deposit layer can be explained by differences in the local concentration and mobility of the deposited primary particles and agglomerates. We have also presented how the latter properties depend upon the parameters of the deposition model.

As a next step, we plan to incorporate the dispersed-phase model proposed in this work into a turbulent pipe-flow solver. This will improve the model correspondence to realistic problem geometries and will allow model predictions to be compared to literature data obtained in cylindrical devices (e.g., to the agglomeration of asphaltene particles in toluene–heptane mixtures, studied in Couette flow cells^{3,4}). Also, two-way coupling will be applied to systems in which deposition occurs, such that, for instance, the dependence of the flow-rate reduction upon the Reynolds number or the asphaltene phase separation rate can be studied. Ultimately, the results that can be obtained using our model should enable the development of improved engineering models, predicting asphaltene deposition under actual oil production conditions.

■ NOTE

All numerical values mentioned throughout this work, as well as the actual model implementations, have been non-dimensionalized using the channel height H , the pressure gradient velocity u_V and the fluid density and viscosity ρ_f and η_f unless noted otherwise. The physical dimensions denoted in the nomenclature are for reference only.

■ ASSOCIATED CONTENT

S Supporting Information

Additional results on the shape of the agglomerates formed in the absence of deposition and re-entrainment for the bending and twisting breakup mechanisms as well as the spatial deposition profiles for $\zeta = 0.5$ and 2.0 and $\gamma = 0.3$ and 0.75. This material is available free of charge via the Internet at <http://pubs.acs.org>.

■ AUTHOR INFORMATION

Corresponding Author

*E-mail: k.c.j.schutte@tudelft.nl.

Notes

The authors declare no competing financial interest.

■ ACKNOWLEDGMENTS

This research was carried out in the context of the Integrated Systems Approach to Petroleum Production (ISAPP) Knowledge Center. ISAPP is a joint project of the Netherlands Organization for Applied Scientific Research (TNO) and Delft University of Technology, sponsored by ENI, Petrobras, and Statoil.

■ NOMENCLATURE

Greek Symbols

α	= wall area covered by deposited particles (%)
γ	= particle–wall interaction scaling coefficient
δ_s	= wall-normal distance to face of particle (m)
δ_w	= average wall-normal coordinate of primary particles
ζ	= damping ratio
η	= viscosity (Pa s)
θ	= diameter-normalized deposit layer thickness
ξ	= particle–wall interaction decay coefficient
ρ	= density (kg/m ³)
τ_p	= particle relaxation time (s)
ϕ	= volume fraction
Ψ	= coefficient vector
Ω	= angular velocity (rad/s)

Latin Symbols

c	= damping constant (N s/m)
D_f	= fractal dimension
F_p	= hydrodynamic force on primary particle (N)
F_{wall}	= particle–wall interaction force (N)
H	= channel height (m)
I	= moment of inertia tensor (kg m ²)
k	= spring constant (N/m)
L	= domain length (m)
m	= mass (kg)
n	= number of grid points
N	= number per unit volume (m ⁻³)
r_p	= position relative to agglomerate center of mass (m)
R_c	= particle–wall interaction range (m)
R_g	= radius of gyration (m)
R_p	= primary particle radius (m)
t	= time (s)
t_{relax}	= relaxation time for particle–wall interaction (s)
T	= torque (N m)
U	= velocity vector (m/s)
u_V	= turbulent flow pressure-gradient velocity (m/s)
W	= wall-normal velocity component (m/s)
x	= streamwise coordinate (m)
y	= spanwise coordinate (m)
z	= wall-normal coordinate (m)

Sub- and Superscripts

∇	= pressure gradient
a	= agglomerate
B	= bending
cm	= center of mass
f	= fluid
L	= bond strength threshold

N = straining
 p = particle
 S = shearing
 T = twisting

Operators

\dot{N} = time derivative of N (s^{-1})
 \tilde{Q} = Q corrected for added mass

- (21) Goldstein, H. *Classical Mechanics*; Addison-Wesley: Boston, MA, 2002.
- (22) Yarranton, H. W.; Masliyah, J. H. Molar mass distribution and solubility modeling of asphaltenes. *AIChE J.* **1996**, *42*, 3533–3543.
- (23) Rahmani, N. H. G.; Dabros, T.; Masliyah, J. H. Settling properties of asphaltene aggregates. *Energy Fuels* **2005**, *19*, 1099–1108.

■ REFERENCES

- (1) Leontaritis, K. J.; Mansoori, G. A. Asphaltene deposition: A survey of field experiences and research approaches. *J. Pet. Sci. Eng.* **1988**, *1*, 229–239.
- (2) Maqbool, T.; Raha, S.; Hoepfner, M. P.; Fogler, H. S. Modeling the aggregation of asphaltene nanoaggregates in crude oil–precipitant systems. *Energy Fuels* **2011**, *25*, 1585–1596.
- (3) Rahmani, N. H. G.; Dabros, T.; Masliyah, J. H. Evolution of asphaltene floc size distribution in organic solvents under shear. *Chem. Eng. Sci.* **2004**, *59*, 685–697.
- (4) Rahimi, H.; Solaimany Nazar, A. R. Asphaltene aggregates fractal restructuring model, a population balance approach. *Energy Fuels* **2010**, *24*, 1088–1093.
- (5) Khoshandam, A.; Alamdar, A. Kinetics of asphaltene precipitation in a heptane–toluene mixture. *Energy Fuels* **2010**, *24*, 1917–1924.
- (6) Escobedo, J.; Mansoori, G. A. Heavy-organic particle deposition from petroleum fluid flow in oil wells and pipelines. *Pet. Sci.* **2010**, *7*, 502–508.
- (7) Jamialahmadi, M.; Soltani, B.; Müller-Steinhagen, H.; Rashtchian, D. Measurement and prediction of the rate of deposition of flocculated asphaltene particles from oil. *Int. J. Heat Mass Transfer* **2009**, *52*, 4624–4634.
- (8) Ramirez-Jaramillo, E.; Lira-Galeana, C.; Manero, O. Modeling asphaltene deposition in production pipelines. *Energy Fuels* **2006**, *20*, 1184–1196.
- (9) Vargas, F. M.; Creek, J. L.; Chapman, W. G. On the development of an asphaltene deposition simulator. *Energy Fuels* **2010**, *24*, 2294–2299.
- (10) Akbarzadeh, K.; Eskin, D.; Ratulowski, J.; Taylor, S. Asphaltene deposition measurements and modeling for flow assurance of tubings and flow lines. *Energy Fuels* **2012**, *26*, 495–510.
- (11) Boek, E. S.; Ladva, H. K.; Crawshaw, J. P.; Padding, J. T. Deposition of colloidal asphaltene in capillary flow: Experiments and mesoscopic simulation. *Energy Fuels* **2008**, *22*, 805–813.
- (12) Ho, C. A.; Sommerfeld, M. Modelling of micro-particle agglomeration in turbulent flows. *Chem. Eng. Sci.* **2002**, *57*, 3073–3084.
- (13) Richardson, D. C. A self-consistent numerical treatment of fractal aggregate dynamics. *Icarus* **1995**, *115*, 320–335.
- (14) Perrine, R. P.; Richardson, D. C.; Scheeres, D. J. A numerical model of cohesion in planetary rings. *Icarus* **2011**, *212*, 719–735.
- (15) Mäkinen, J. T. T. Particle accretion and dissipation simulator: Collisional aggregation of icy particles. *Icarus* **2005**, *177*, 269–279.
- (16) Chen, D.; Doi, M. Microstructure and viscosity of aggregating colloids under strong shearing force. *J. Colloid Interface Sci.* **1999**, *212*, 286–292.
- (17) Portela, L. M.; Oliemans, R. V. A. Eulerian–Lagrangian DNS/LES of particle–turbulence interactions in wall-bounded flows. *Int. J. Numer. Methods Fluids* **2003**, *43*, 1045–1065.
- (18) Li, Y.; McLaughlin, J. B.; Kontomatis, K.; Portela, L. Numerical simulation of particle-laden turbulent channel flow. *Phys. Fluids* **2001**, *13*, 2957–2967.
- (19) Schutte, K. C. J.; Portela, L. M.; Henkes, R. A. W. M. A numerical study on the formation and break-up of particle agglomerates. *Proceedings of the 8th International Conference on Multiphase Flow*, Jeju, South Korea, May 26–31, 2013; Paper 731.
- (20) Hollander, E. D.; Derkxen, J. J.; Portela, L. M.; van den Akker, H. E. A. Numerical scale-up study of orthokinetic agglomeration in stirred vessels. *AIChE J.* **2001**, *47*, 2425–2440.